Final Report 03/06/2015

Project Title: Providing Diurnal Sky Cover Data at ARM Sites
Institution: Solmirus Corporation
Street Address/City/State/Zip: 1044 Elkton Dr./Colorado Springs/CO/80907
Postal Address: 3532 Spruce Road/Woodland Park/CO/80863
Principal Investigator: Dr. Dimitri Klebe/719.964.3838/dklebe@solmirus.com
Administrative Point of Contact: Dimitri Klebe/719.964.3838/dklebe@solmirus.com
DOE/Office of Science Program Office: Biological and Environmental Research (BER)
DOE/Office of Science Program Office Technical Contact: Dr. Ashley Williamson
DOE Grant Number: DE-SC-0008650
Research Area: Climate and Environmental Sciences

Final Report:

1. Introduction

The Solmirus Corporation was awarded two-year funding by the U.S. Department of Energy (Grant No. DE-SC-0008650) to perform a comprehensive data analysis of observations made during Solmirus' 2009 field campaign (conducted from May 21 to July 27, 2009 at the ARM SGP site) using the All Sky Infrared Visible Analyzer (ASIVA) instrument. The objective was to develop a suite of cloud property data products for the ASIVA instrument that could be implemented in real time and tailored for cloud modelers. This final report describes our research and findings enabled by this grant. Much of this research as well as details of ASIVA's calibration procedures has been published in the article *"Ground-based all-sky mid-infrared and visible imagery for purposes of characterizing cloud properties"*. This article is available from the peer-viewed online journal Atmospheric Measurement Techniques. (http://www.atmos-meas-tech.net/7/637/2014/amt-7-637-2014.html) An ASIVA instrument was recently purchased for the ARM SGP site. The instrument, referred to as IRSI (Infrared Sky Imager), has been in operation since May 2014. Several data products developed under this grant have been implemented for the IRSI instrument and refinement of the data analysis procedures enabled by this grant is ongoing.

2. Sky Cover

2.1 Robust retrieval of Sky Cover data product from ASIVA IR dataset

The primary objective of this award was to develop a diurnal sky cover (SC) data product utilizing the ASIVA's infrared (IR) radiometrically-calibrated data. ASIVA's unique infrared capabilities rest on its utilization of an all-sky lens. Coupled with calibration procedures, this enables the successful removal of clear-sky emission. The basic procedure in distinguishing clouds from clear-sky emission and determining sky cover is illustrated in figures 1 and 2.

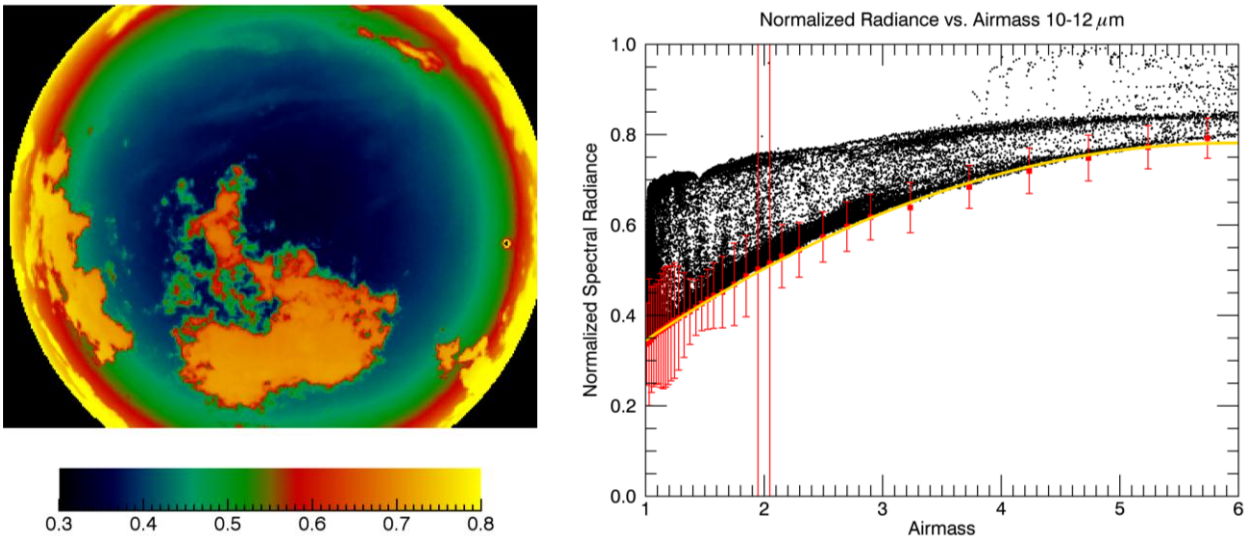

Figure 1: a) Normalized radiance image. b) Pixel normalized radiance vs. airmass data. Gold line represents 2nd-order polynomial fit to lower envelope of points (red squares) in each of 35 airmass bins and denotes the clear-sky emission.

Figure 1a shows a radiometrically-calibrated image in units of normalized radiance (i.e. the radiance has been divided by the radiance of the blackbody reference) obtained in ASIVA's 10.2-12.2 μm filter. Calibrated images are analyzed by plotting the radiance vs. airmass (figure 1b) enabling the determination of a lower radiance envelope due to the water vapor continuum.

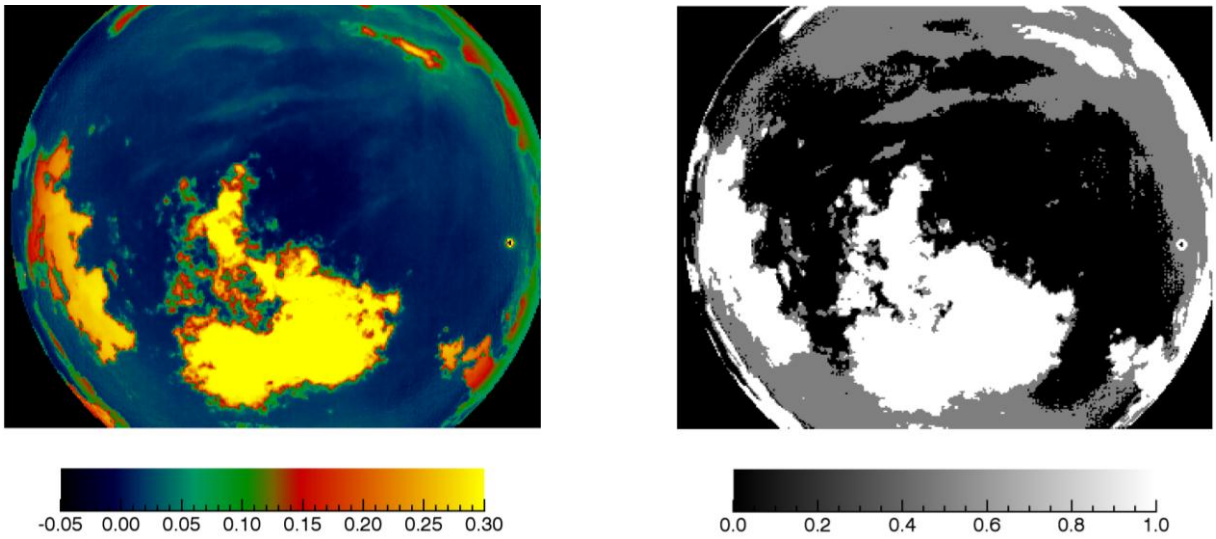

Figure 2: a) Clear-sky subtracted image. b) Cloud mask generated from clear-sky subtracted image utilizing two thresholds for high-emission (white) and low-emission (grey) clouds.

A polynomial fit of the clear-sky radiance as a function of airmass is used to subtract the clear-sky radiance from the normalized radiance image yielding the cloud structures in excess of this clear-sky emission (figure 2a). Properly identifying the clear-sky continuum has historically been the Achilles heel of infrared sky imaging systems. Without this ability it becomes extremely difficult to distinguish low emission clouds from the water vapor continuum. Cloud threshold levels were selected to generate a cloud decision map (i.e. cloud mask) identifying high-emission (HE) and low-emission (LE) clouds (figure 2b). The radiometrically calibrated data, along with airmass plots and cloud masks for the entire 2009 campaign are compiled in the data files supplied with this report.

One of the primary challenges of producing a robust cloud decision map was determining the clear-sky radiance in nearly 100% cloudy conditions. This was accomplished by first demanding that the chi-square value for the polynomial fit to the clear-sky radiance be less than some threshold (chosen to be 0.01 in this analysis) to ensure a strict goodness-of-fit criterion. If this criterion was not met, the previous polynomial equation that met this criterion was used to define the clear-sky radiance. Figure 3 illustrates cloudy conditions (SC = 75%) in which this chi-square criterion is surprising still met. Note that the fit denotes the proper clear-sky radiance for this image.

In the case of 100% cloudy conditions, the goodness-of-fit criterion could often be met due to an evenly emitting cloud layer. Therefore an additional criterion was put in place to handle this case. If the clear-sky normalized radiance at 1.0 airmass was calculated to be greater than 0.5, then the previous polynomial equation to meet both criteria was used to define the clear-sky radiance. A case in which the sky is nearly 100% cloudy is illustrated in figure 4. Note once again that the fit denotes the proper clear-sky radiance for this image. A very similar procedure

has been implemented for the ARM IRSI instrument.

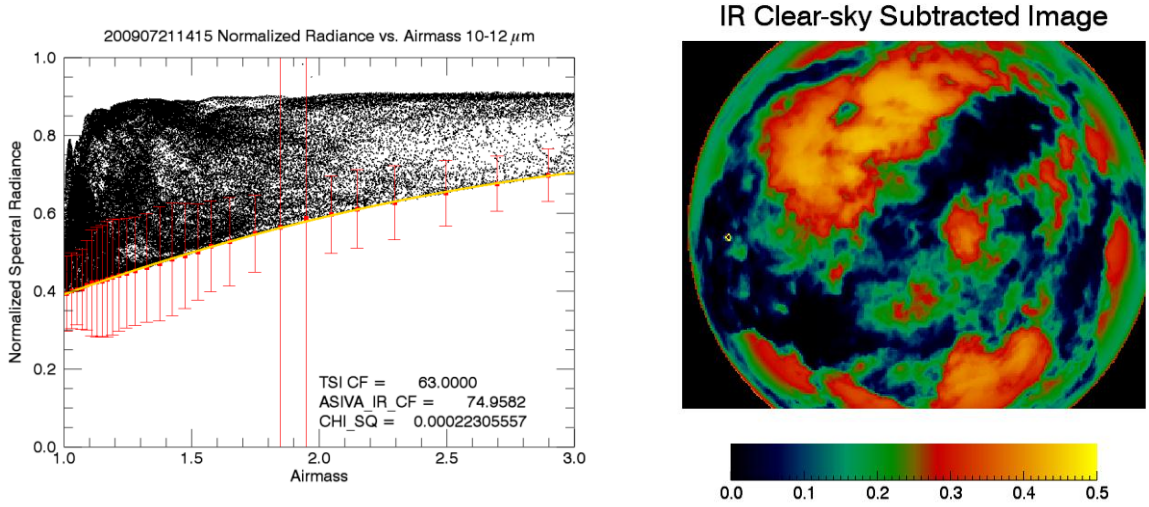

Figure 3: a) Pixel normalized radiance vs. airmass data. Gold line represents 2nd-order polynomial fit to lower envelope of points (red squares) in each of 29 airmass bins. b) Clear-sky subtracted image based on analysis shown in a). Image truncated at six airmasses.

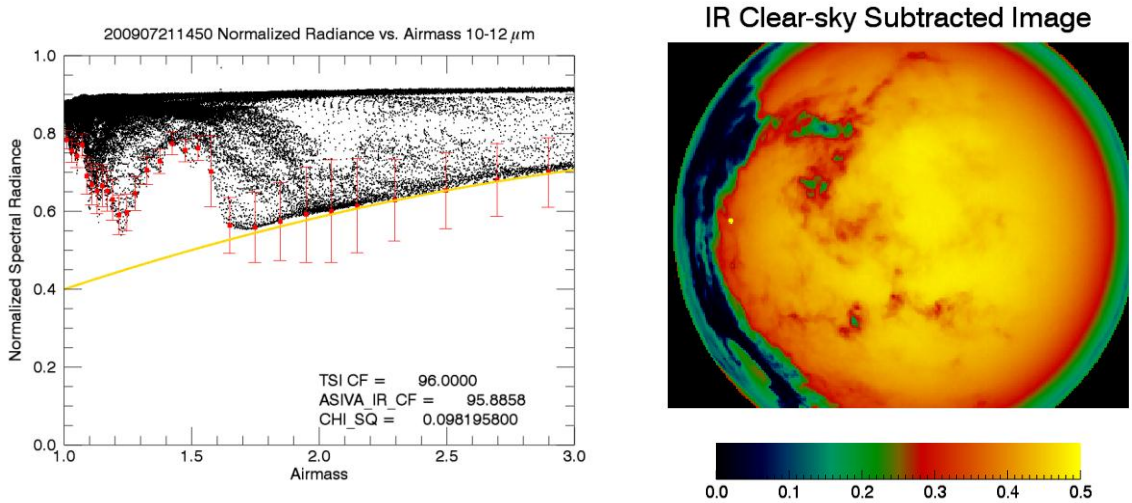

Figure 4: a) Pixel normalized radiance vs. airmass data. Gold line represents 2nd-order polynomial fit to lower envelope of points obtained from the previous dataset that met the chi-square criterion. b) Clear-sky subtracted image based on analysis shown in a).

Research was conducted to determine threshold values that most closely correlated with the opaque and thin cloud designations of the Total Sky Imager (TSI) instrument, which was in operation at SGP during the 2009 field campaign. SC values were determined within a 120-degree cone angle, which closely matched the field-of-view used for by the TSI. Figure 5 shows the results of this comparison applying the adopted threshold values (in normalized radiance units) of $0.03 < LE\ cloud < 0.05$ and $HE\ cloud \geq .05$ to the clear-sky subtracted images. As seen in figure 5a, no correlation was found between the between ASIVA's low emission clouds and TSI's thin cloud designation, which speaks to the fact that the cloud decision analysis is fundamentally different between the IR and visible. However as shown in figure 5b, a good

correlation was measured between ASIVA's high emission clouds and TSI's opaque cloud designation.

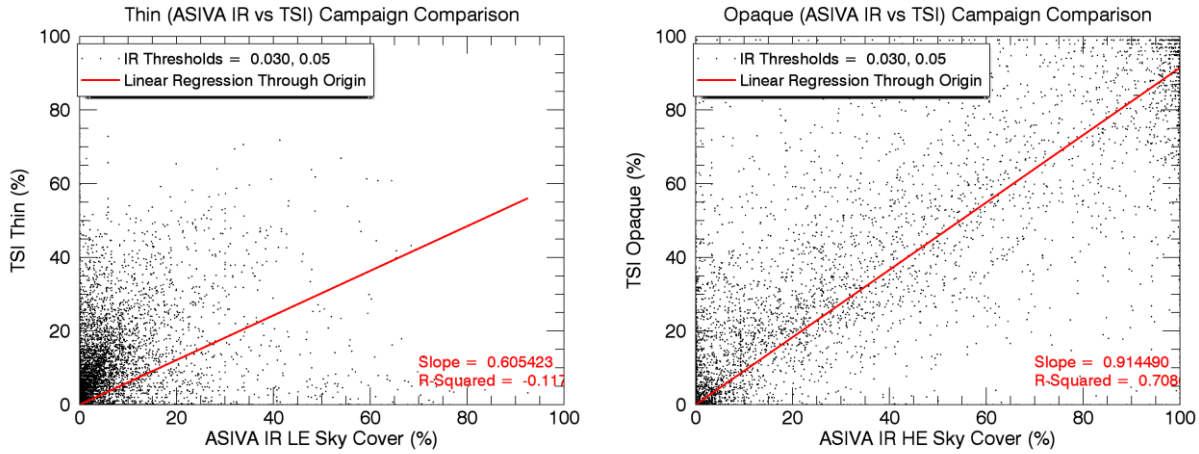

Figure 5: a) Sky cover comparison between TSI and ASIVA IR for thin vs. low emission cloud types and opaque vs. high emission cloud types.

2.2 Robust retrieval of Sky Cover data product from ASIVA Visible dataset

Retrieval of the SC data product from ASIVA's visible channels mimics the analysis adopted by the TSI instrument. The procedure involves taking the ratio of the red image to blue image and then setting appropriate clear/thin and thin/opaque thresholds. As was the case for the infrared channel, SC values for the visible channel were determined within a 120-degree cone angle.

Thresholds where chosen to provide the best agreement with the TSI instrument for the campaign period. Figure 6 shows the results of this comparison applying the adopted threshold values of $0.66 < \textit{thin cloud} < 0.71$ and $\textit{opaque cloud} \geq 0.71$ to the red-to-blue ratio images.

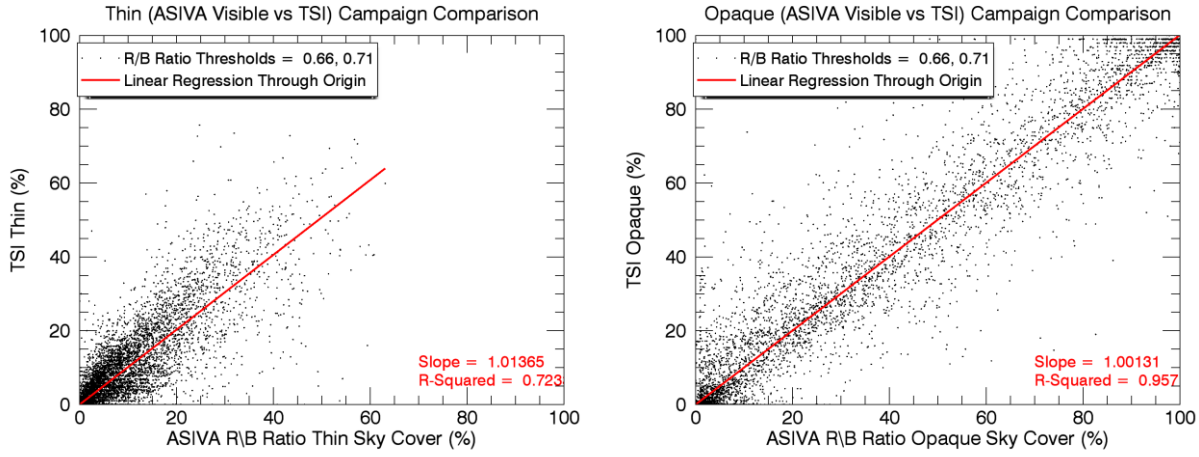

Figure 6: a) Sky Cover comparison between TSI and ASIVA Visible for thin cloud types and b) opaque cloud types.

The correlation is very good and demonstrates that the ASIVA visible subsystem functioned very similarly to the TSI.

2.3 Sky Cover data for 2009 data set

The sky cover data for each 5-minute ASIVA data set have been combined with data from the TSI instrument into a single graphic (referred to as a panel plot) for purposes of comparing the sky cover data products issued from the ASIVA and TSI instruments. An example of a panel plot is given in figure 7. Panel plots for the entire 2009 campaign are compiled in the data files supplied with this report.

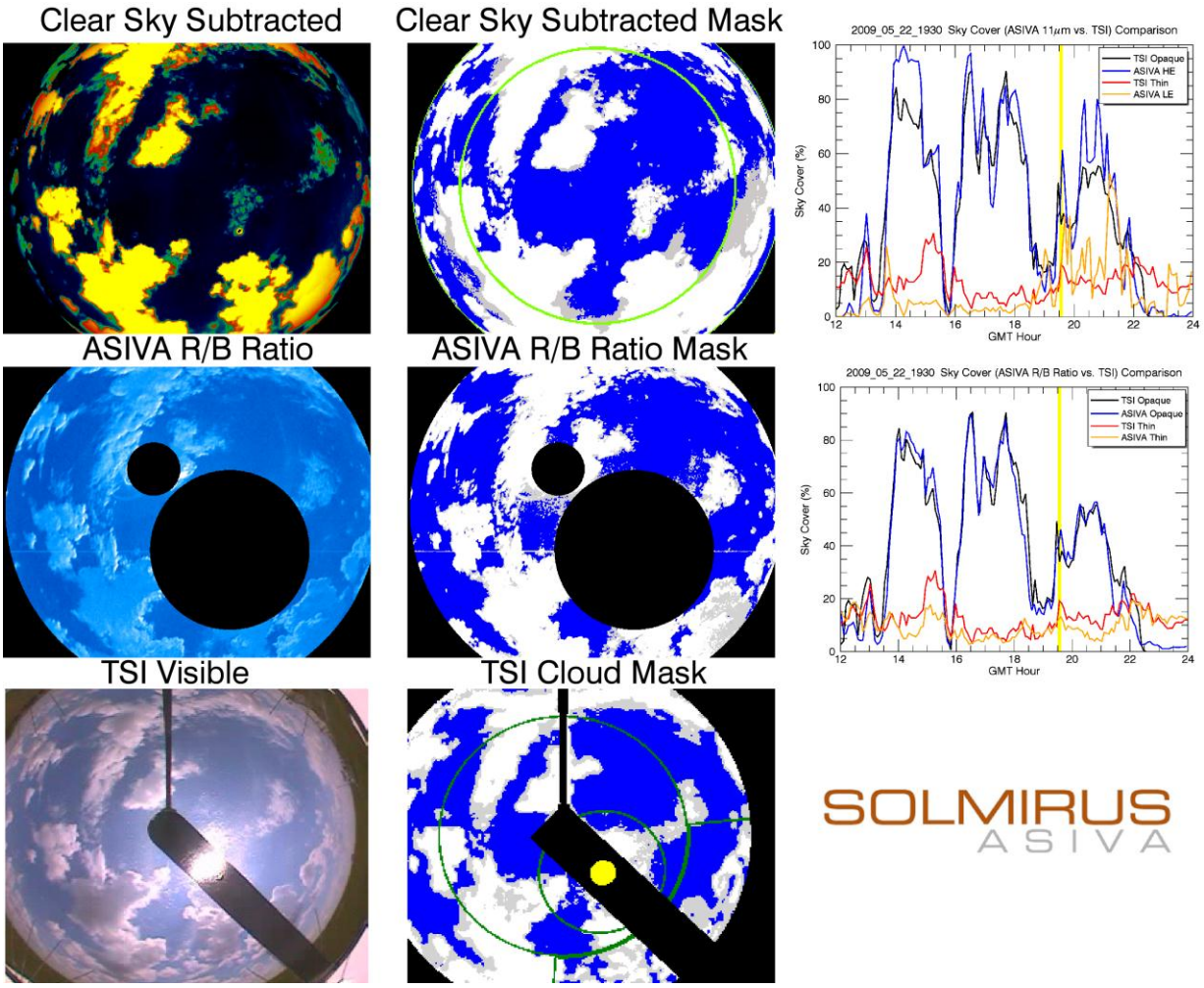

Figure 7: Panel plot for May 22, 2009 GMT 19:32 a) Top row: Clear-sky subtracted normalized radiance, ASIVA IR cloud mask (high emission, low emission, and clear-sky shown in white, grey, and blue respectively), and sky cover comparison plot with TSI data for May 22 (GMT 19:32 is indicated by yellow vertical line in this plot). b) Middle row: ASIVA R/B ratio image, ASIVA visible cloud mask (opaque, thin, and clear-sky shown in white, grey, and blue respectively), and sky cover comparison plot with TSI data for May 22. c) Bottom row: TSI visible image and cloud mask.

3. ASIVA AERI Comparison

In an effort to validate ASIVA calibration procedures, data was retrieved and analyzed from the Atmospheric Emitted Radiance Interferometer (AERI) instrument. Data was retrieved from the entire 2009 campaign from the ARM archive. The mean spectral radiance in each of the two ASIVA IR channels was determined by averaging the AERI data over the ASIVA instrument response in each filter as illustrated in figure 8.

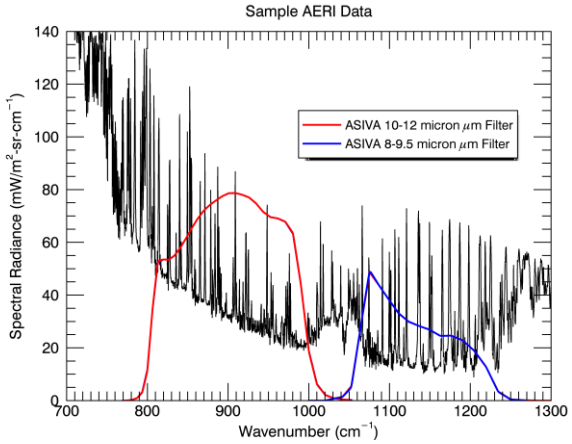

Figure 8: Sample AERI data (black line) and ASIVA's 10.2-12.2 µm (red line) and 8.25-9.25 µm (blue line) instrument response for which the AERI spectral radiance data was averaged.

The 8-minute average AERI data were utilized, as this cadence was similar to the 5-minute cadence used by the ASIVA instrument. Calibrated ASIVA data was then evaluated at the zenith, coincident with AERI's field-of-view. Comparison of AERI data with ASIVA data for two sample days is shown in figure 9. Agreement is very good (<5%) for the two comparisons shown and is representative of the entire campaign dataset. Note that the agreement good in both clear and cloudy circumstances.

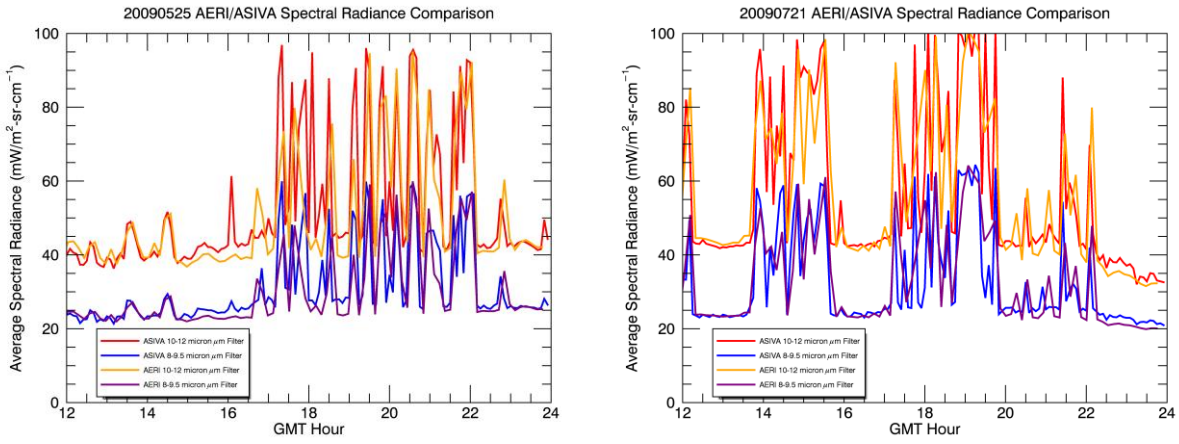

Figure 9: Comparison of AERI with ASIVA spectral radiance data in each of the two filters for May 25, 2009 (left) and July 21, 2009 (right).

In studying the ASIVA AERI comparison data, we often observed a systematic offset between the ASIVA and AERI data. We believe the offset is introduced in the system by cooling

and heating of the IR lens between the hatch-open and hatch-closed position respectively. Current ASIVA instruments (this includes the ARM IRSI instrument) now incorporate an external blackbody to combat this issue. For purposes of this research, we used knowledge of this offset to better calibrate the data (referred to as offset corrected) for purposes of more accurately determining the other cloud property data products discussed in this report.

4. Precipitable Water Vapor (PWV) Determination

Determination of precipitable water vapor (PWV) is important as it can provide valuable ancillary information in the analysis of other cloud property data products. The basic analysis strategy was to compare the clear-sky emission (determined from the SC analysis and shown in figure 1b) with that derived from modeled data. The model data was constructed using a series of MODTRAN simulations that provided a parameterization of the normalized clear-sky downwelling radiance as a function of PWV evaluated at different elevation angles (i.e. airmass). In addition, the models were run for a variety of visibility conditions for the purposes of future research. The data presented here adopts a constant visibility factor. Simulations were run for each of ASIVA's filters using a standard mid-latitude summer atmosphere at sea level and a lapse rate extracted from a radiosonde dataset acquired for July 21, 2009. The simulated dataset is then best fit to the clear-sky emission determined for a particular image in each of the filters thus providing an estimate of PWV. For this research, we looked at two different methods for determining the best fit to the MODTRAN data. The first method minimized the total magnitude of the difference between the ASIVA and modeled data. This method was therefore most sensitive to the overall level of the clear-sky emission. The second method minimized the total standard deviation of the difference between the ASIVA and modeled data. This method was therefore most sensitive to the shape of the clear-sky emission as a function of airmass. Figure 10 shows the result of this analysis for the May, June, and July datasets. The PWV data is compared with that retrieved from the Microwave Radiometer (MWR), an instrument with accuracy of better than 1 mm PWV.

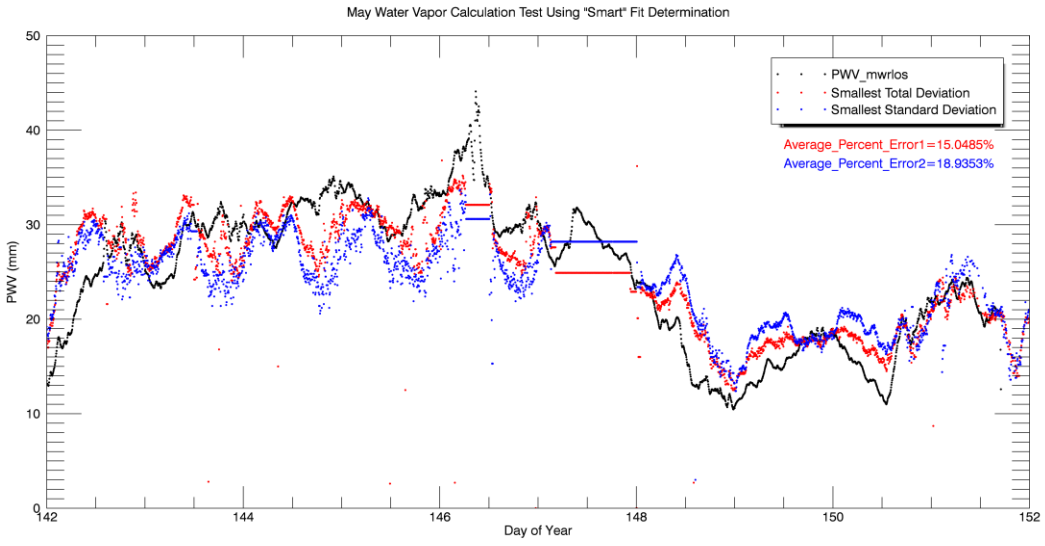

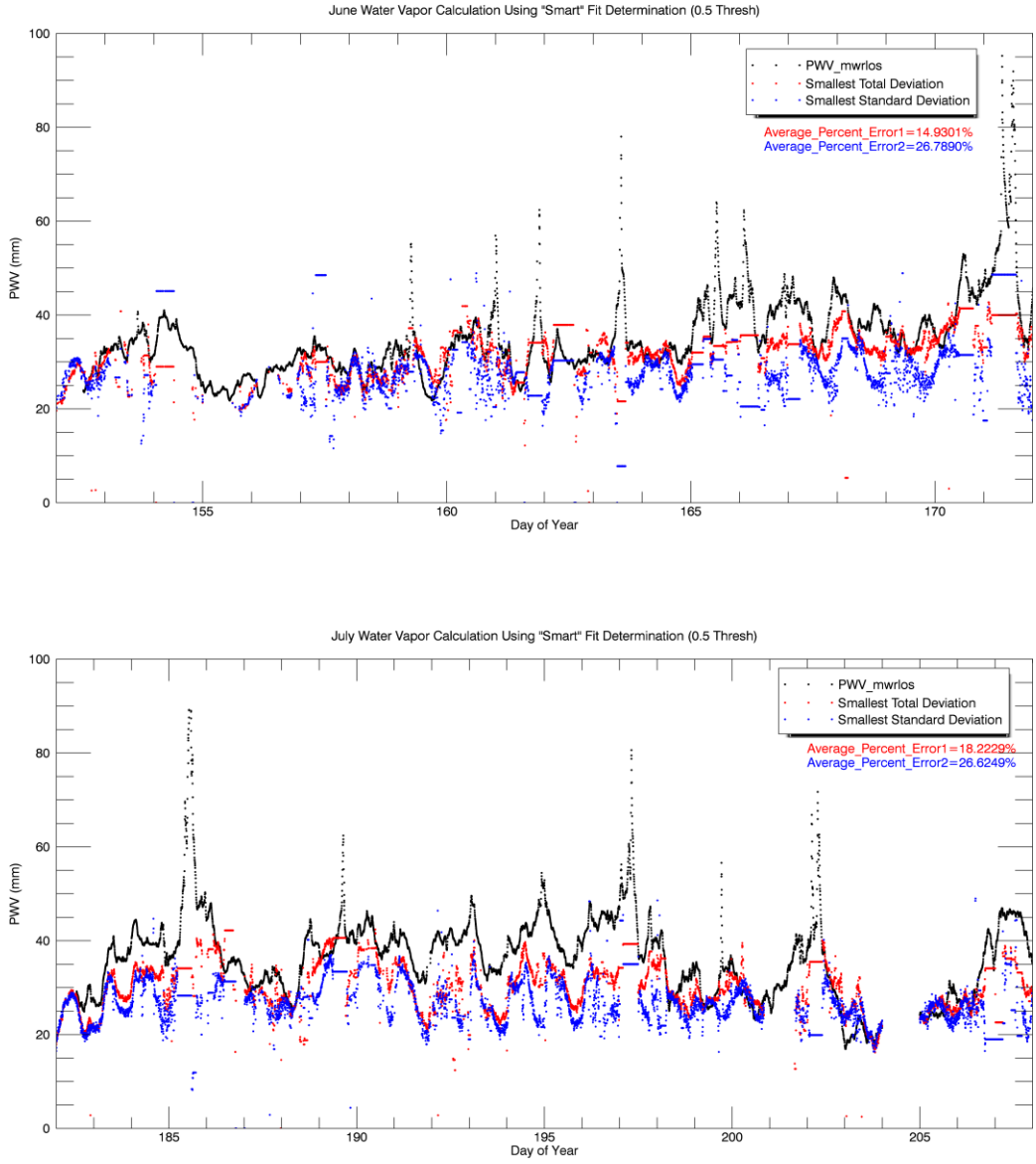

Figure 10: Comparison of Microwave Radiometer (PWV_mwrlos) with ASIVA PWV data for May (top), June (middle) and July, 2009 (bottom).

As can be seen from figure 10, this method does a fair job of assessing atmospheric PWV. Periods of constant PWV (horizontal lines in figure 10) are due to very cloudy conditions were the clear-sky emission could not be determined (i.e. the sky was very cloudy and the clear-sky envelope could not be evaluated) and was thus assumed to be constant. In general, the method minimizing total deviation provides a more accurate measure (~16% error on average) than the method of minimizing the standard deviation (~25% error on average). Improving our calibration and modeling is an ongoing process to better determine PWV with the ASIVA instrument.

5. Determination of Cloud Temperature

Two temperature data products can be immediately derived from ASIVA's calibrated IR radiance data: brightness temperature and color temperature. The brightness temperature (for a given IR filter) of the image can be determined by equating the measured radiance with a blackbody whose temperature yields this same radiance. Two examples of brightness temperature images are shown in figure 11. Note that the peripheries of the clouds indicate lower brightness temperature consistent with lower optical depth in these regions.

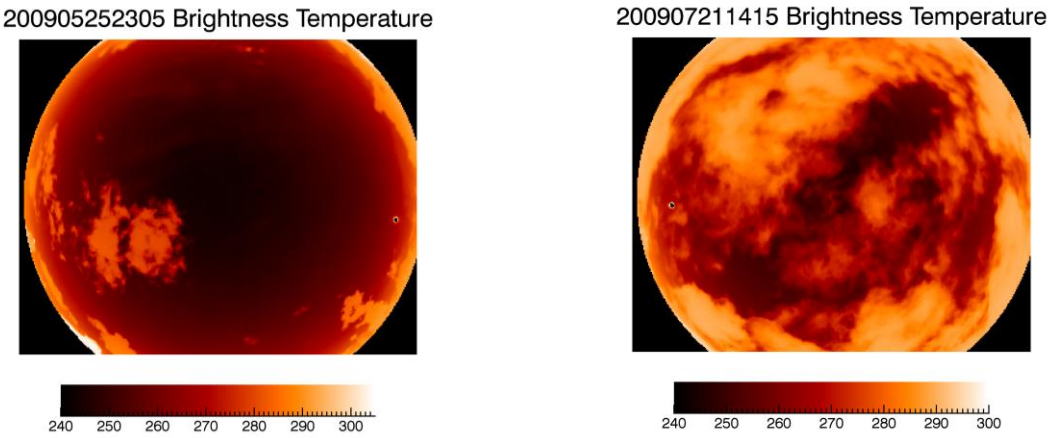

Figure 11: Brightness temperature (K) for representative images on May 25, 2009 (left) and July 21, 2009 (right).

The color temperature can be inferred by taking the ratio of the sky radiance images acquired in the 8.25-9.25 μm and 10.2-12.2 μm filters and equating this to the a blackbody temperature that yields this same radiance ratio. Color temperature has the distinct advantage of only being affected by differences in cloud emissivity in the two filters but not to the total optical depth. For this reason we believe that color temperature ultimately yields a better measure of the true temperature for optically thin clouds. Color temperature images are shown in figure 12.

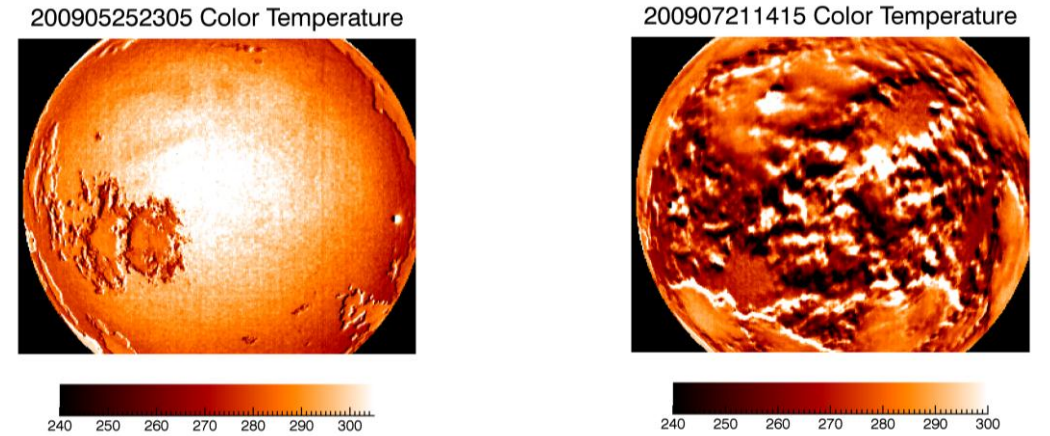

Figure 12: Color temperature (K) for representative images on May 25, 2009 (left) and July 21, 2009 (right).

Both of the images in figure 12 show variations (both positive and negative temperature

fluctuations) at the periphery of the clouds due to the motion of the clouds over the data acquisition period. This is particularly evident in the July 21st image as the clouds were very fast moving. Current ASIVA instruments now acquire 8.25-9.25 µm and 10.2-12.2 µm image data in a much shorter time interval to combat this problem. Also note that the clear-sky color temperature is brighter at the zenith due to sky emissivity differences in the two IR filters.

Color temperatures in the optically thick regions of clouds shown in figure 11 are consistent with those of figure 12 and both indicate cloud temperatures 10-20 K below the ground temperature. Color temperature images for the entire 2009 campaign are compiled in the data files supplied with this report.

6. Determination of Cloud Height

We also investigated the potential of providing cloud height information from the ASIVA IR data. Our approach was to assign a cloud height based on its temperature (both brightness and color). To do this, radiosonde data for the entire 2009 campaign period was retrieved from the ARM archive. The temperature vs. altitude data was fit with a polynomial equation, which was then used to derive a cloud height from the cloud temperature data. Derived cloud height data was then compare with ceilometer data also retrieved from the ARM archive. Cloud height data along with other important data products derived from the ASIVA instrument are presented in the comprehensive data plots of figure 13.

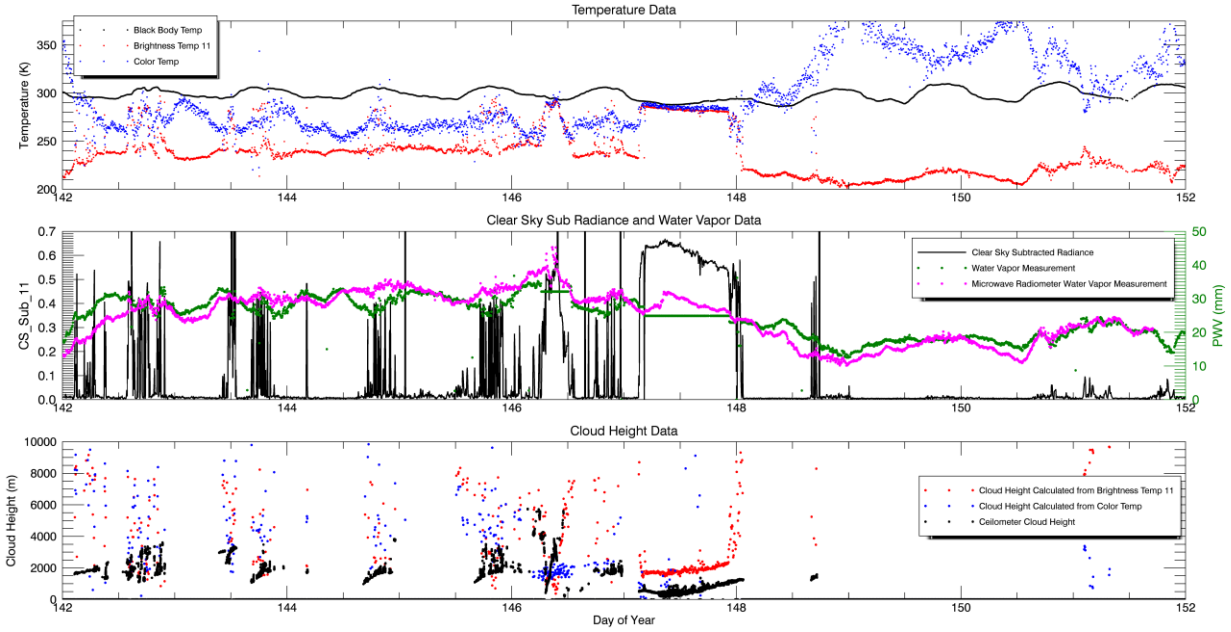

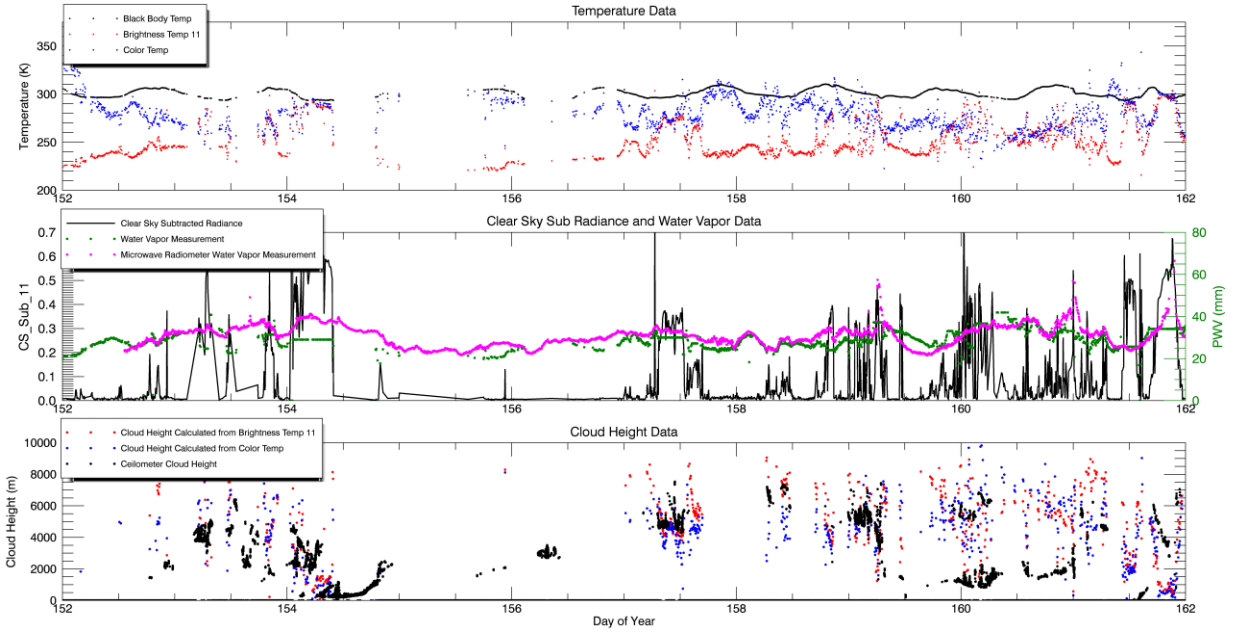
Temperature Data
Black Body Temp
Brightness Temp 11
Color Temp
Temperature (K)
Clear Sky Sub Radiance and Water Vapor Data
Clear Sky Subtracted Radiance
Water Vapor Measurement
Microwave Radiometer Water Vapor Measurement
CS_Sub_11
PWV (mm)
Cloud Height Data
Cloud Height Calculated from Brightness Temp 11
Cloud Height Calculated from Color Temp
Ceilometer Cloud Height
Cloud Height (m)
Day of Year

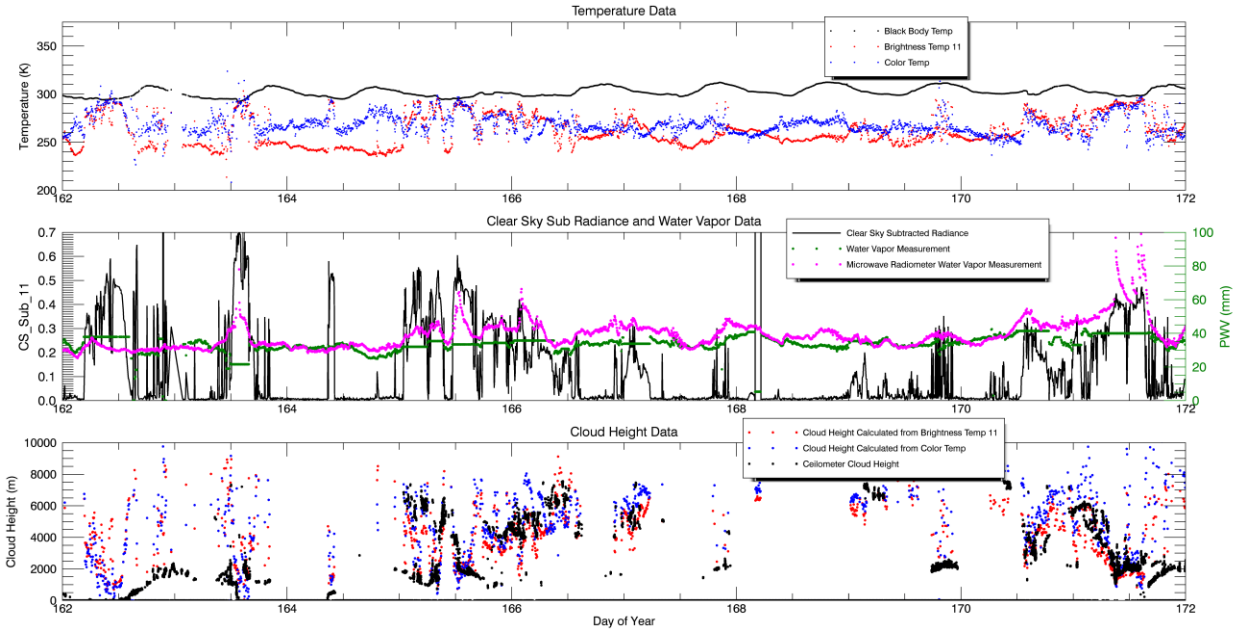
Temperature Data
Black Body Temp
Brightness Temp 11
Color Temp
Temperature (K)
Clear Sky Sub Radiance and Water Vapor Data
Clear Sky Subtracted Radiance
Water Vapor Measurement
Microwave Radiometer Water Vapor Measurement
CS_Sub_11
PWV (mm)
Cloud Height Data
Cloud Height Calculated from Brightness Temp 11
Cloud Height Calculated from Color Temp
Ceilometer Cloud Height
Cloud Height (m)
Day of Year

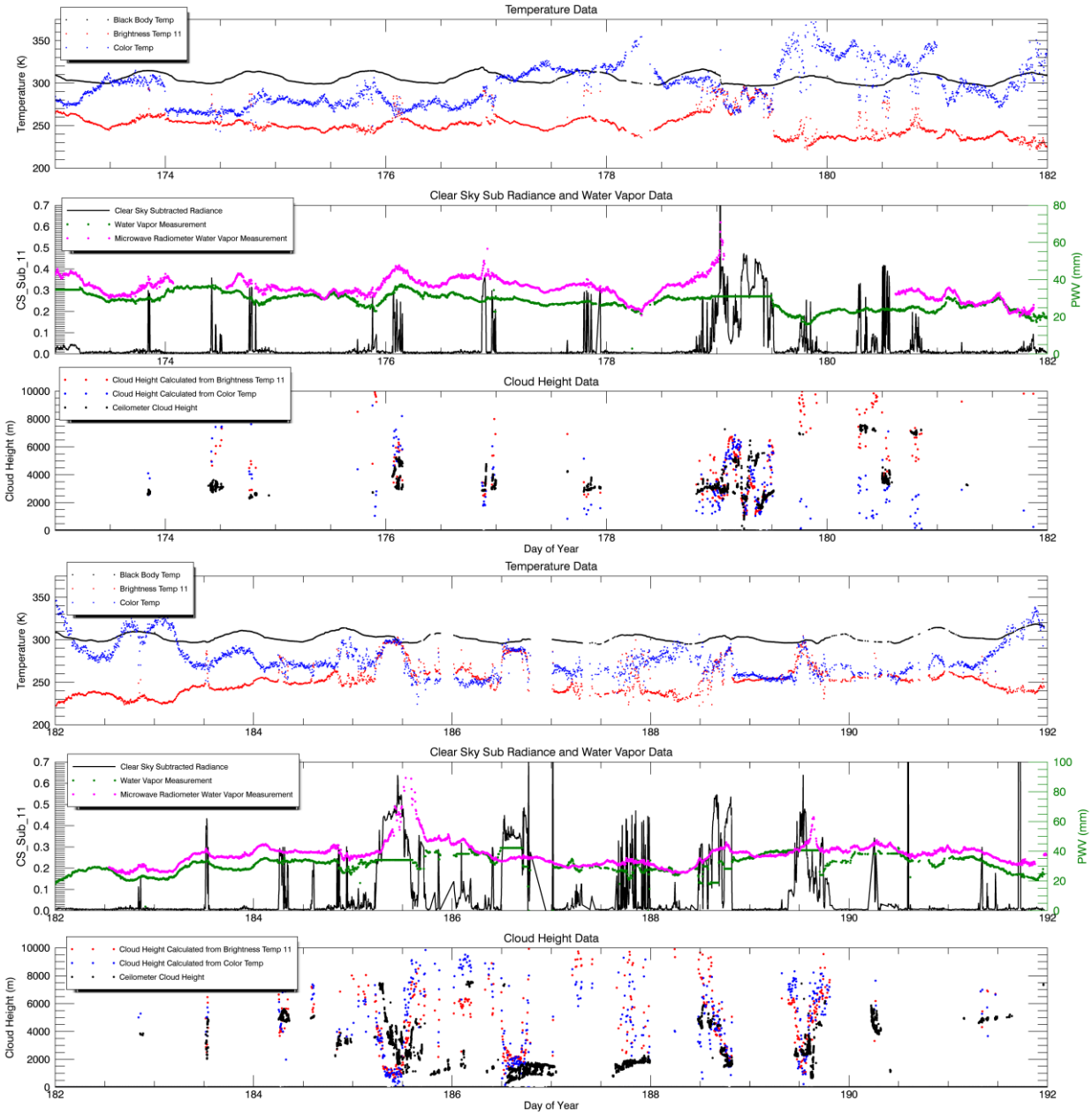
Temperature Data
Black Body Temp
Brightness Temp 11
Color Temp
Temperature (K)
Clear Sky Sub Radiance and Water Vapor Data
Clear Sky Subtracted Radiance
Water Vapor Measurement
Microwave Radiometer Water Vapor Measurement
CS_Sub_11
PWV (mm)
Cloud Height Data
Cloud Height Calculated from Brightness Temp 11
Cloud Height Calculated from Color Temp
Ceilometer Cloud Height
Cloud Height (m)
Day of Year

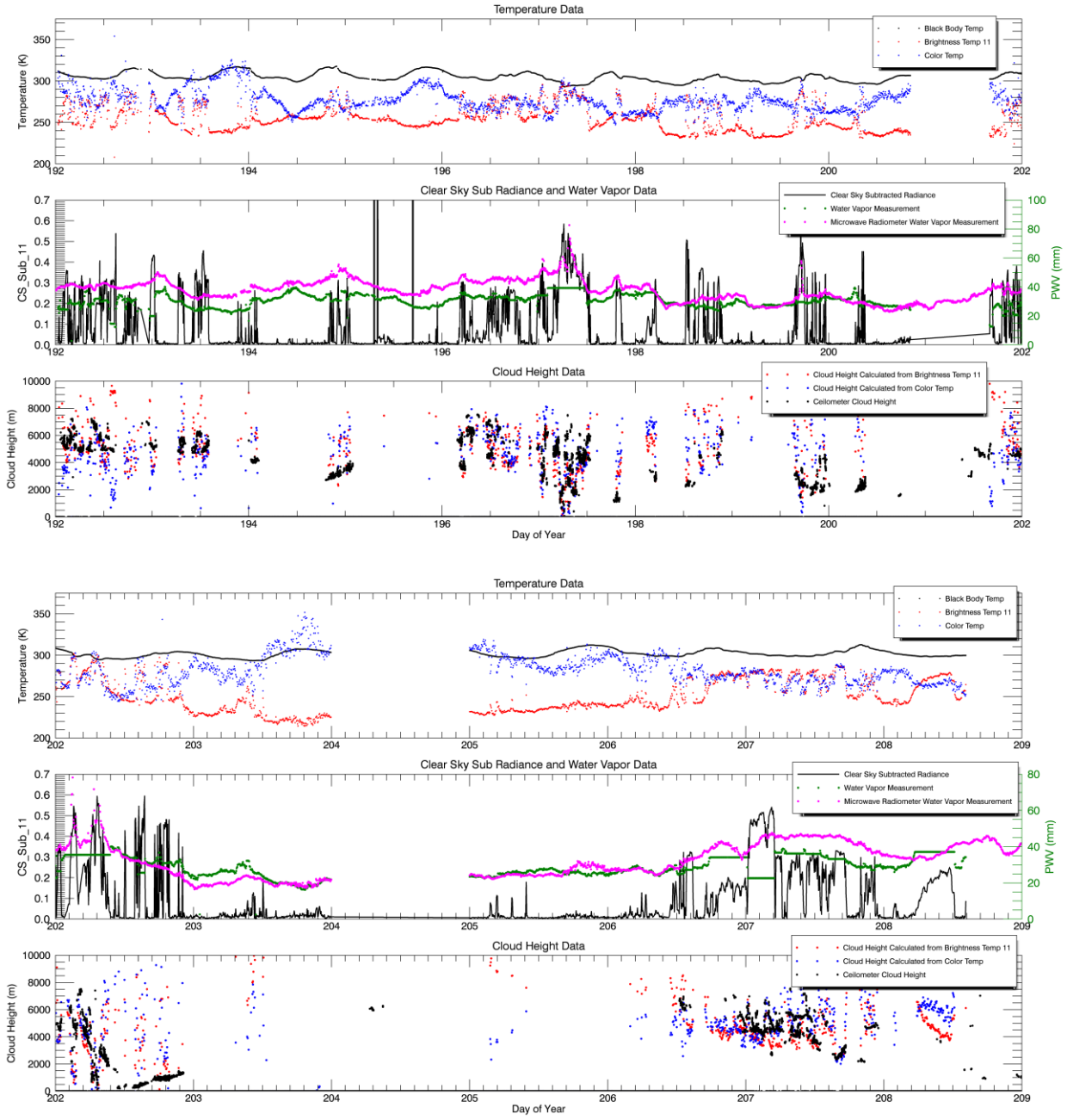

Figure 13: Comprehensive data plots for entire 2009 data set (day 142-209). Top panel: Comparison of blackbody temperature (i.e. ground temperature) with brightness and color temperature evaluated at the zenith. Middle panel: Comparison of clear sky subtracted normalized radiance (evaluated at the zenith) with PWV determined from the ASIVA and Microwave Radiometer instruments. Bottom panel: Comparison of cloud height determined from cloud brightness and color temperatures with cloud heights reported from ceilometer.

The top plot of figure 13 illustrates that brightness temperature and color temperature generally converge to the same value (~10-30 K below the ground temperature) during cloudy conditions. During clear conditions the sky brightness temperature is considerably lower (~30-80 K below

the ground temperature) as expected due to the lower emissivity of the sky. The color temperature, however, lies closer to the ground temperature (generally within ~30 K) but can vary both positively and negatively from the ground temperature. This variance does not seem to be correlated with PWV and at present we do not have a good explanation for this behavior. The middle plot reproduces the PWV data described earlier in this report along with the clear-sky subtracted normalized radiance evaluated at the zenith. The clear-sky radiance indicates whether or not clouds are present. The bottom plot shows the comparison of cloud height data. In general the cloud height determined from temperature data is higher than that reported from the ceilometer. This is somewhat expected in that the ceilometer reports cloud bottom height and the temperature of a cloud is assessed at a point within the cloud where the cloud becomes optically thick. However there are other time periods in which there was good correlation between the different cloud height measures.

The cloud height comparisons shown in figure 13 do not provide a compelling argument that cloud height can be reliably determined from cloud temperature data. We then turned our attention to see if we might fine a correlation between the clear-sky subtracted normalized radiance and cloud height. Figure 14 shows the results of this analysis.

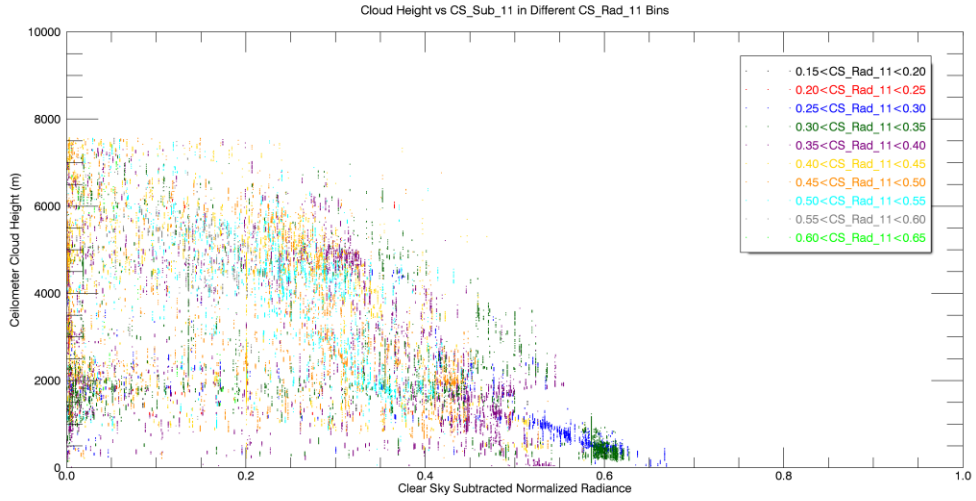

Figure 14: Plot for entire 2009 data set of cloud height reported from the ceilometer versus the cloud's clear-sky subtracted normalized radiance evaluated at the zenith. Colors indicate clear-sky radiance range for a particular observation and are indicative of the amount of water vapor present.

Figure 14 shows a provocative correlation between these two parameters. The plot shows a roughly linear correlation that runs from 7,000 meters and zero radiance down to zero meters and 0.65 clear-sky subtracted normalized radiance. However there is also a horizontal spur that extends along ~2,000 meter elevation. We are still trying to grasp the meaning of this result and this is the subject of our future research. Though it does not look promising that the ASIVA will be able to determine cloud height from its radiance data, we believe the variance may be due to cloud thickness and/or optical depth variations. We are currently running Modtran simulations to see if we can replicate this result and whether or not it provides insight to determining cloud thickness and/or optical depth.

6. 2009 Campaign Data

The processed data from the entire 2009 campaign can be accessed from Solmirus' server **data.solmirus.com** using username (armdata) and password (Solmirus01). Under the main data directory there is the AsivaData directory, which contains the following subdirectories.

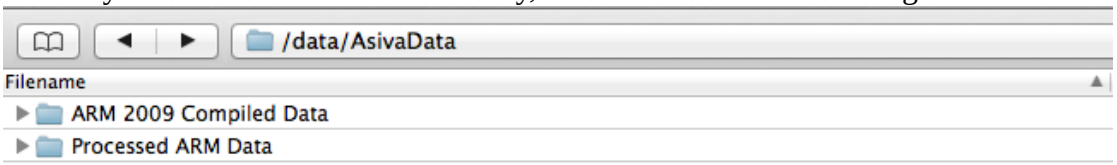

Under the subdirectory "ARM 2009 Compiled Data" one will find the following files and folders. Of primary interest, this subdirectory contains some of the plots highlighted in this report.

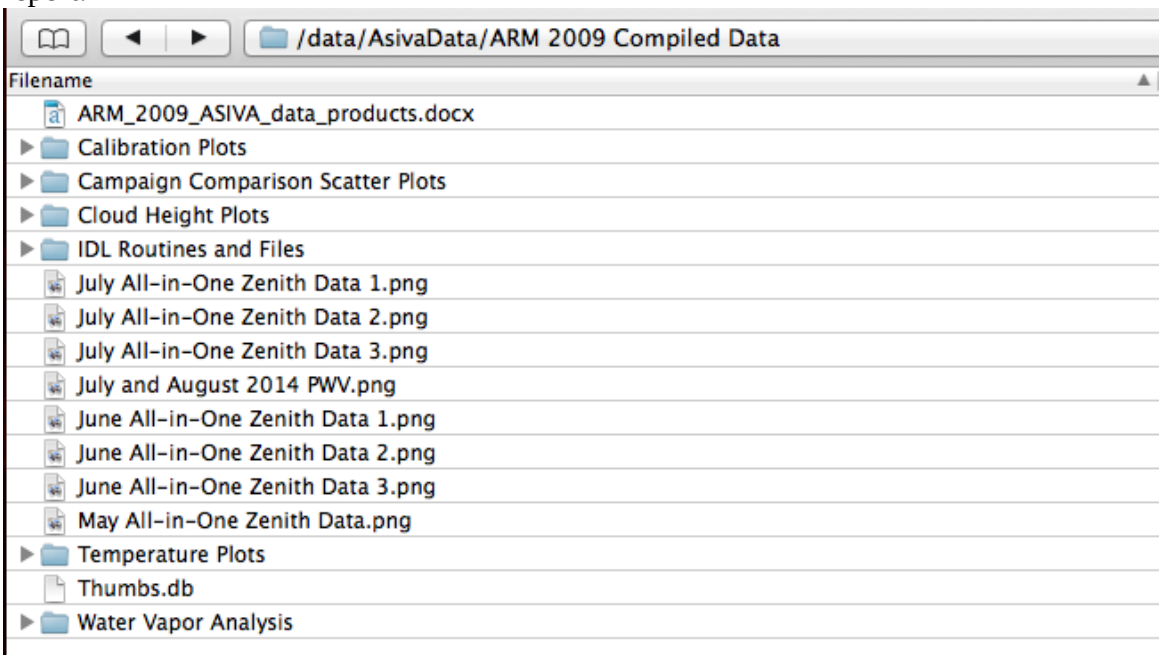

Under the "Processed ARM Data" subdirectory all processed data is contained in the day's appropriate folder for each day of the field campaign.

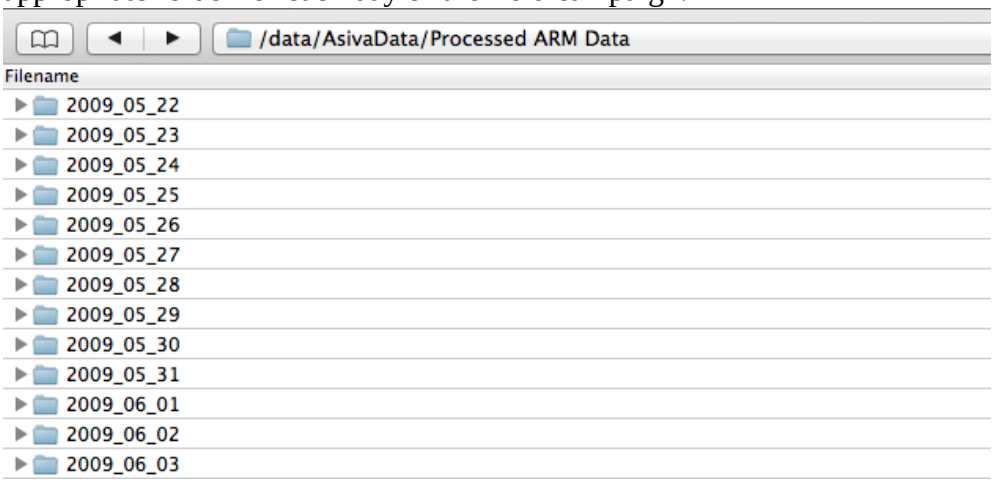

Each day's folder contains the following data folders.

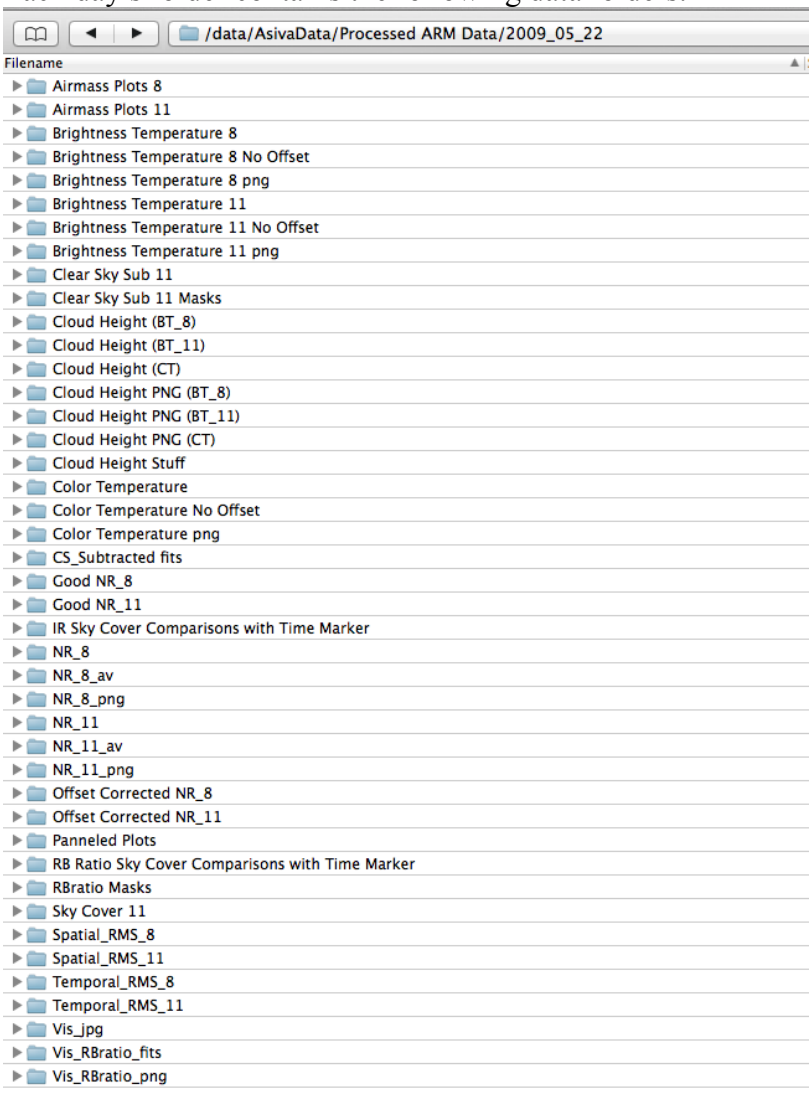

The processed data within these folders is described below.

Airmass Plots 8: 8-9 µm airmass plots created with a max normalized radiance threshold (0.5)/good chi squared value (0.01) clear sky detection method.
Airmass Plots 11: 10-12 µm airmass plots created with a max normalized radiance threshold (0.5)/good chi squared value (0.01) clear sky detection method.
Brightness Temperature 8: 8-9 µm Brightness Temperature FITS images.
Brightness Temperature 8 png: 8-9 µm Brightness Temperature png images.
Brightness Temperature 11: 10-12 µm Brightness Temperature FITS images.
Brightness Temperature 11 png: 10-12 µm Brightness Temperature png images.
Clear Sky Sub 11: 10-12 µm clear sky subtracted radiance FITS images created with a max normalized radiance threshold (0.5)/good chi squared value (0.01) clear sky detection method.
Cloud Height (BT_8): 8-9 µm cloud height FITS images derived from 8-9 µm brightness temperature.

Cloud Height (BT_11): 10-12 μm cloud height FITS images derived from 10-12 μm brightness temperature.
Cloud Height (CT): Cloud height FITS images derived from color temperature.
Cloud Height PNG (BT_8): 8-9 μm cloud height png images derived from 8-9 μm brightness temperature. Note, error in title, should be "Cloud Height from BT_8".
Cloud Height PNG (BT_11): 10-12 μm cloud height png images derived from 10-12 μm brightness temperature. Note, error in title, should be "Cloud Height from BT_11".
Cloud Height PNG (CT): Cloud height derived from color temperature png images.
Color Temperature: Color temperature FITS images derived from the 8-9μm to 10-12μm radiance ratio.
Color Temperature png: Color temperature png images derived from the 8-9μm to 10-12μm radiance ratio.
CS_Subtracted 11: 10-12 μm clear sky subtracted radiance FITS images created with a good chi squared value clear sky detection method.
Good NR_8: Good (offset corrected using AERI data comparison) 8-9 μm normalized radiance FITS images.
Good NR_11: Good 10-12 μm normalized radiance FITS images.
NR_8: 8-9 μm normalized radiance data for ~0.5 second integration in FITS format.
NR_8_av: 8-9 μm normalized radiance data for ~8 second integration in FITS format.
NR_8_png: 8-9 μm normalized radiance data png images.
NR_11: 10-12 μm normalized radiance data for ~0.5 second integration in FITS format.
NR_11_av: 10-12 μm normalized radiance data for ~8 second integration in FITS format.
NR_11_png: 10-12 μm normalized radiance data png images.
Offset Corrected NR_8: 8-9 μm normalized radiance data corrected with an offset derived from comparison with AERI data in FITS format.
Offset Corrected NR_11: 10-12 μm normalized radiance data corrected with an offset derived from comparison with AERI data in FITS format.
Sky Cover 11: 4 plots depicting daily sky cover.
Spatial_RMS_8: 8-9 μm Spatial Root-Mean-Square images in FITS format.
Spatial_RMS_11: 10-12 μm Spatial Root-Mean-Square images in FITS format.
Temporal_RMS_8: 8-9 μm Temporal Root-Mean-Square images in FITS format.
Temporal_RMS_11: 10-12 μm Temporal Root-Mean-Square in FITS format.
Vis_jpg: Visible jpg images.
Vis_RBratio_fits: Visible Red/Blue ratio in FITS format.
Vis_RBratio_png: Visible Red/Blue ratio png images.